Quantum description of a charged plasmonics nanowire dimer

Dan Xiang,[1] Hong Zhang,[1,*] Lorenzo Stella,[2,3,†] and Fan Yang[1,‡]

[1]*College of Physics and Key Laboratory of High Energy Density Physics and Technology of the Ministry of Education, Sichuan University, Chengdu, Sichuan 610065, China*

[2]*Centre for Light-Matter Interactions (CLMI), School of Mathematics and Physics, Queen's University Belfast, University Road, Belfast BT7 1NN, United Kingdom*

[3]*School of Chemistry and Chemical Engineering, Queen's University Belfast, Stranmillis Road, Belfast BT9 5AG, United Kingdom*

(Received 1 January 2024; revised 10 May 2024; accepted 14 May 2024; published 6 June 2024)

The charging effect has been a ubiquitous phenomenon in our daily lives. Here, we investigate the role played by this effect in a prototype nanowire dimer structure with an *ab initio* density-functional approach. Various charging configurations for the nanowire dimer have been explored, showing that the excess charge strongly modulates the ground and excited state. Furthermore, the opposite charging of the nanowire dimer breaks the symmetry of electron distribution and potential barrier, facilitating the formation of a charge-transfer current through the gap.

DOI: 10.1103/PhysRevB.109.245407

I. INTRODUCTION

The charging effect is a universal electrostatic phenomenon in daily life [1]. There are two kinds of charges, positive and negative, where the like charges repel and the unlike charges attract. These phenomena stimulated the discovery of Coulomb's law, laying the foundation of electromagnetic theory [2,3]. Electrostatic interaction plays a leading role in the nanoscale, making investigating the charging effect of great significance in unveiling the fundamental nature of physics.

Plasmonic materials featuring a high density of conduction electrons are ideal candidates for exploring charging effects. Owing to the unique possibility of overcoming the diffraction limit and enhancing a local electric field, the properties of plasmonic materials [4] have been extensively explored, especially the enhancement of the electric field of plasmonic nanostructure [5]. Plasmonic devices that have been fabricated and investigated experimentally include nanolasers [6], optical sensors [7], photocatalytic and electrochemical nanostructures [8,9], etc. The optical response of a plasmonic nanostructure is typically dictated by its geometry, material properties, and environment. Recent development in electrochemical modulation has facilitated the active control of plasmonic excitation and response [10–12]. For instance, Byers *et al.* have demonstrated an extreme and reversible change in scattering line shape by oxidation-reduction chemistry [11]. On the other hand, biasing a nanogap within a plasmonic nanostructure also facilitates reversible control of its optical response by fine-tuning the tunneling conductance [13–15].

Alternatively, the optical response of a plasmonic nanostructure can be tuned by local charging, i.e., by locally increasing or decreasing the unperturbed electronic density [16,17]. Such local changes result in uncompensated local charges that can substantially affect the surface potential barrier and the overall electric potential, resulting in a giant frequency shift of the plasmonic response from the neutral (i.e., compensated) case [18]. To account for the local charging effect in plasmonic nanostructures, density functional theory (DFT) [19,20] and time-dependent density functional theory (TDDFT) [21–25] have been applied to model the response of a charged plasmonic nanostructure and cluster [16,17,26–28]. To the best of our knowledge, the response of a charged plasmonic dimer has yet to be investigated.

In this paper, we utilize DFT and TDDFT to study the charging effects in a plasmonic nanowire dimer, a widely used prototype of plasmonic nanostructure [29–34]. To explore various combinations of charging configurations, a method of applying static and then time-evolving external potential is proposed to generate the charged nanowire dimer. Three kinds of charged nanowire dimers are investigated: (1) two wires are both positively charged; (2) both negatively charged; (3) two wires are oppositely charged. Compared with the neutral counterpart, the additional charge induces giant modulations of ground and excited states.

II. METHOD

Our *ab initio* calculations for the nanowire dimer system are based on DFT and TDDFT as implemented in the OCTOPUS code [35–37]. DFT is first utilized to calculate the Kohn-Sham potential and charge density of the ground state. Then, real-time TDDFT is used to calculate the frequency-resolved optical absorption cross section following the application of an impulsive perturbation, or a "delta-kick," in the electric field, $E_0\delta(t)$, polarized along the nanowire dimer axis [38]. Local density approximation has been used

*hongzhang@scu.edu.cn
†l.stella@qub.ac.uk
‡fyang@scu.edu.cn

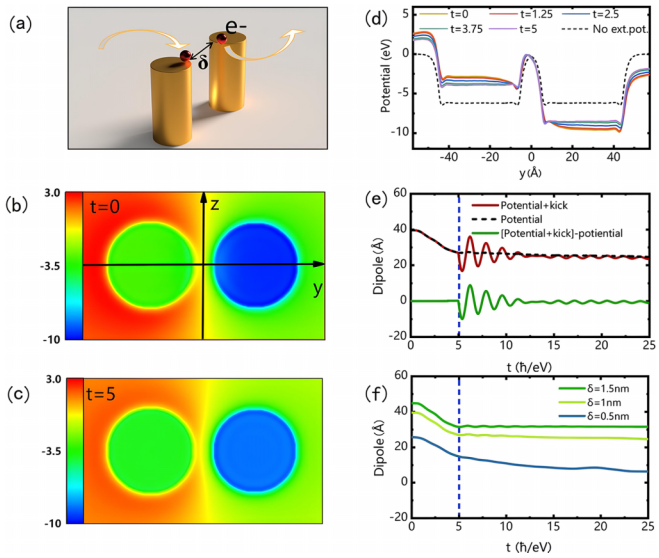

FIG. 1. Method for studying the charged plasmonic system. (a) The nanowire dimer system considered in this paper. (b) Initial Kohn-Sham potential at $t = 0$. (c) Kohn-Sham potential at $t = 5$ in the unit of $\hbar$/eV. (d) Kohn-Sham potential along the y axis. Solid curves diagram the temporal evolution of potential when the external field smoothly diminishes from initial maximum to zero at $t = 5$ $\hbar$/eV, compared with the case of without scalar potential illustrated as a black dashed line. (e) Temporal evolution of induced dipole. Dashed black curve: only external potential is added. Brown solid curve: delta kick is immediately applied when potential vanishes at $t = 5$ $\hbar$/eV. Solid green curve: the temporal evolution of induced dipole contributed only by the applied impulsive perturbation. (f) Time evolution of dipole moment for the nanowire dimer with different gaps.

for the exchange-correlation potential in DFT and TDDFT calculations [39].

The jellium model [38,40] is employed to describe a plasmonic dimer made up of two parallel nanowires directed along the x axis, as shown in Fig. 1(a). The Wigner-Seitz radius is $r_s = 4a_0$, where a_0 is the Bohr radius, corresponding to sodium, which is a prototypical free electron metal [41]. The simulation cell is a parallelepiped with periodic boundary conditions applied along the longitudinal direction of the nanowires, while Dirichlet boundary conditions are applied to the transverse directions. The extension of the simulation cell along the periodic direction is parametrized as h [32]. The centers of the nanowires lie on the y axis and the length of the gap between them is indicated as δ. Within the jellium model, the positive background density of sodium is defined as $n_{ion} = 3/4\pi r_s^3$ and the nanowire radius and period are set as $R = 2$ nm and $h = 0.7679$ nm, so to accommodate 256 electrons for each nanowire in the periodic simulation cell.

For an overall positively (negatively) charged dimer, the OCTOPUS package allows removing (adding) a given number of electrons from the system. Regarding an overall neutral dimer with opposite charging of the two nanowires, we resorted to a different preparation. First, we introduce a static "hyperbolic tangent" scalar potential into the ground state calculation to polarize the dimer by transferring, e.g., one electron from the right to the left wire. This static potential

TABLE I. Parameter setting for the static potential in Eq. (1).

δ	c_0	Excess electron (left)	Excess electron (right)
0.5 nm	0.6	1	−1
1 nm	0.9	1	−1
1.5 nm	1	1	−1

is defined as

$$V_{\text{sta}} = \frac{2c_0}{h}\tanh\left(\frac{y}{\delta}\right), \tag{1}$$

where c_0 is the parameter used to tune the charge transfer between the two wires.

The "hyperbolic tangent" scalar potential is then gently removed during a short real-time TDDFT propagation, leaving the two nanowires oppositely charged in the absence of any static external field. The time-dependent external field employed to remove the initial static polarization reads

$$V_{\text{ext}}(t) = V_{\text{sta}}(0.016t^3 - 0.12t^2 + 1)H(5 - t), \tag{2}$$

where $H(t)$ is the Heaviside step function, and the temporal evolution factor smoothly transits from 1 at $t = 0$ to 0 at $t = 5$ $\hbar$/eV. The Kohn-Sham potential distribution at these two times is shown in Figs. 1(b) and 1(c), respectively.

To glimpse this removal process, we compare the potential distributions along the dimer axis at different intermediate times between $t = 0$ and $t = 5$ $\hbar$/eV in Fig. 1(d). A clear transition of the potential from oblique to flat inside the nanowires can be observed. This is an evidence that the effects of the initial polarization have been removed and the charge density has equilibrated inside the nanowires. Compared to the case without external potential (black dashed line), the potential barrier in the gap between the nanowires becomes asymmetric when two nanowires are oppositely charged.

After the external potential has vanished at $t = 5$ $\hbar$/eV, we can evaluate the number of electrons that have been transferred before studying the optical response. The total number of transferred electrons is evaluated by integrating the electron density in each nanowire. Table I summarizes the values of the parameter c_0 selected for transferring one electron from the right nanowire to the left one at $t = 5$ $\hbar$/eV, for different gap sizes.

After the external potential function has vanished at $t = 5$ $\hbar$/eV, an impulsive perturbation or a delta-kick is immediately applied, allowing us to calculate the frequency-resolved optical absorption cross section using a longer TDDFT propagation (40 $\hbar$/eV). The induced dipole of the nanowire dimer with (red line) and without (black dashed line) the impulsive perturbation is reported in Fig. 1(e). The time evolution of the case without delta-kick shows that the induced dipole becomes stationary, demonstrating that a net dipole moment has been established due to transferred charges. If the delta-kick is applied, the dipole oscillates around the value of this net dipole moment due to the electronic excitations, including the plasmon mode. To isolate the contribution from electronic excitations, we subtract the baseline dipole evolution without the delta-kick from the dipole evolution following a delta-kick. The result of this operation is indicated as $P(t)$ and shown as the green line in Fig. 1(e).

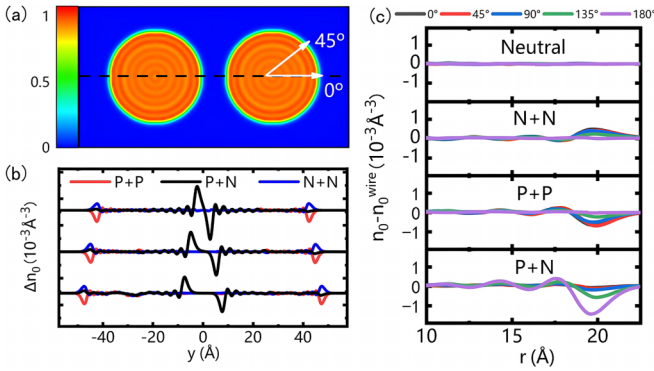

FIG. 2. Charge distribution of ground state. (a) Charge density of the neutral dimer. (b) Change of electron density, Δn_0, distribution along the dimer axis [dashed line in panel (a)] compared with neutral dimer. Top curves: $\delta = 0.5$ nm; middle: $\delta = 1$ nm; bottom: $\delta = 1.5$ nm. (c) Electron density of neutral, negatively, positively, and oppositely charged dimer at different angles of the right nanowire [defined as the white arrow in panel (a)] when gap size is 1 nm. The data in panel (c) has been subtracted by the electron density of an isolated neutral nanowire.

From the time evolution of dipole moment $P(t)$ purely due to the impulsive perturbation, we can evaluate the dipole polarizability along the dimer axis as

$$\alpha(\omega) = \frac{1}{E_0}\int P(t)e^{i\omega t-\gamma t}dt, \tag{3}$$

where a numerical damping factor γ has been introduced and set to 0.1 eV/ħ. Then, the frequency-resolved absorption cross section is given by [38]

$$\sigma(\omega) = \frac{4\pi\omega}{c}\mathrm{Im}[\alpha(\omega)]. \tag{4}$$

We have also investigated how gap size δ changes the induced dipole evolution in time. In Fig. 1(f), three distinct gap sizes are considered when gently removing the initial polarization. A large gap size (1 nm and 1.5 nm) is associated with a stationary dipole moment after the initial polarization has been removed. On the other hand, a smaller gap like $\delta = 0.5$ nm results in a nonstationary dipole moment, decreasing after the removal of the initial polarization. This finding can be explained as charge transferring back by tunneling across the gap between the two nanowires, making the dipole moment of the dimer smaller over time.

III. RESULTS

Let us first consider the nanowire dimer's ground state with different charging configurations and gap sizes. Figure 2(a) shows the electron distribution of a neutral nanowire dimer. In the jellium model, the electron distribution, n_0, smoothly decreases from its average bulk value, n_{ion}, to zero across the nanowire boundary. Oscillations around the average value are analog to the Friedel oscillations due to the sharp edge of the jellium background. To illustrate how charging effects modulate the electron distribution, we plot the change of electron density, Δn_0, along the dimer axis [dashed line in Fig. 2(a)]. Δn_0 is defined as the difference between the electron density of the charged and neutral nanowire dimer. Three cases are shown in Fig. 2(b): both nanowires positively charged (P + P); both nanowires negatively charged (N + N); oppositely charged nanowires (P + N). Three sets of curves are reported for different gap sizes (0.5 nm, 1 nm, and 1.5 nm from top to bottom, respectively). Figure 2(b) shows that the access charge tends to localize at the metal surface rather than in the bulk region, which can be explained by the Gauss theorem of electrostatics. The access charge is compensated in the bulk region to restore neutrality. When two nanowires are charged with like charges (P + P and N + N), the access charge tends to localize at the left and right ends of the dimer structure. In contrast, in the P + N case, Δn_0 localizes close to the gap. These findings can be rationalized as electrostatic repulsion in the P + P and N + N or electrostatic attraction in the P + N case. Note that electrostatic attraction between unlike charges results in the large modulation of electron density close to the gap.

In Fig. 2(c), electron density along a radial direction for the right nanowire is shown for different angles. For the sake of high contrast between different cases, all electron distributions have been subtracted by that of an isolated neutral nanowire, whose electron distribution is angle independent due to symmetry. The results shown in Fig. 2(c) confirm that the electron density of the neutral nanowire dimer is angle independent, i.e., a uniform distribution along the boundary. This is not the case for charged nanowire dimers. For the P + P and N + N cases, the distribution of Δn_0 decreases as the angle is increased, while in the P + N case, the opposite trend is observed. Therefore, the additional charges on the two nanowires interact via Coulomb's law, resulting in a nonuniform distribution on the surface of the nanowire dimer.

The physical significance of Fig. 2(c) can be further revealed in the framework of the Feibelman d parameter [40,42]. The parameter $d_\parallel$ quantizes the surface charging, which is usually assumed to be uniform along the surface [43]. It can be defined by n_0 as

$$d_\parallel = \int \frac{n_0(r) - n_j}{n_{ion}}dr, \tag{5}$$

where n_0 represents the electron density of the ground state and n_{ion} (n_j) is the density of ion (jellium) density. The integration is along the direction normal to the metal interface which for the nanowire is along the radial direction. The results in Fig. 2(c) demonstrate that n_0 varies for different angular directions, such that an angle-dependent $d_\parallel(\theta)$ should be employed instead to characterize the surface charging according to Eq. (5). The $d_\parallel$ vanishes for the charge-neutral nanowire dimer as a result of uniform charge distribution along the metal surface and charge conservation. However, $d_\parallel$ becomes nontrivial for the charged structure as shown in Fig. 3. Figures 3(b)–3(d) illustrate the d parameter of charged nanowire dimer for $\delta = 1.5$ nm, $\delta = 1$ nm, and $\delta = 0.5$ nm, respectively. For the P + P and N + N cases, the d parameter is calculated only for one nanowire due to the symmetry. Since the number of electrons removed in the P + P case is the same as that added in the N + N case, the d parameter of the P + P case is nearly the opposite number of the N + N case. On the

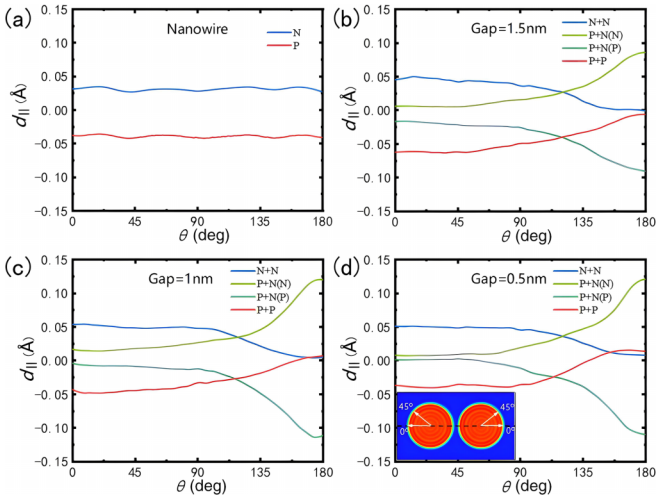

FIG. 3. d parameter ($d_{\parallel}$) as a function of the angle of different kinds of charging configurations for different gap distances. (a) d parameter of a single nanowire. (b) 1.5 nm; (c) 1 nm; (d) 0.5 nm. The inset shows how the angle is defined in the dimer system.

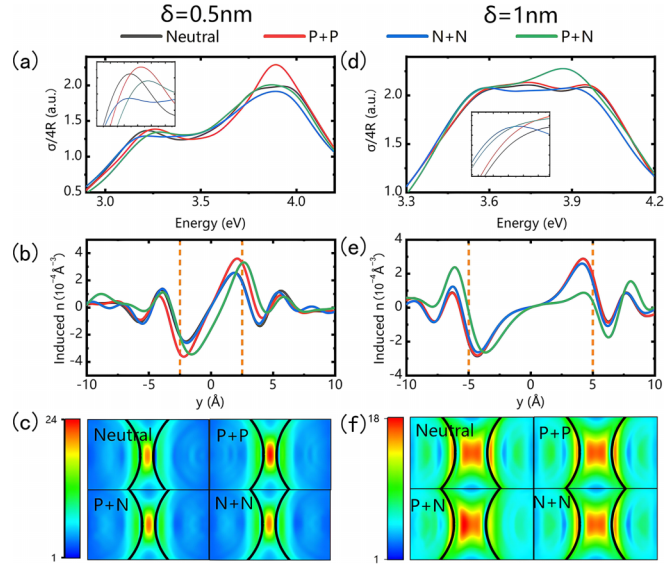

FIG. 4. Excited states of charged nanowire dimers with different gaps and charging configurations. (a), (d) Absorption spectrum of the charged dimer. The inset shows the magnifying regions around the absorption peaks. The first resonance frequency reads 3.226 eV (neutral), 3.263 eV (P + P), 3.221 eV (N + N), 3.288 eV (P + N) for the case $\delta = 0.5$ nm and 3.56 eV (neutral), 3.562 eV (P + P), 3.55 eV (N + N), 3.53 eV (P + N) for the case $\delta = 1$ nm. (b), (e) Induced charge density at the first resonance. The dashed orange lines represent jellium boundaries. (c), (f) Electric field enhancement near the gap region of the nanowire dimer.

other hand, for the oppositely charged nanowire dimer, the d parameters of both two wires are shown in Figs. 3(b)–3(d). As a result of charge symmetry, the d parameters of the left and the right wires are nearly opposite.

The d parameters of identically and oppositely charged dimers also exhibit discrepancies. The d parameter of P + N configuration varies much more rapidly than that of the P + P and N + N cases. This is attributed to the fact that the excess charges of the P + N case are more localized near the gap region. Moreover, the $d_{\parallel}$ of the identically (oppositely) charge dimer almost vanishes at $\theta \to 180^{\circ}$ ($\theta \to 0^{\circ}$), as a consequence of Coulomb interaction.

In Fig. 3, we also investigate the role of gap distance in the d parameter. From Fig. 3(a) to Fig. 3(d), we gradually decrease the gap size, where Fig. 3(a) corresponds to $\delta \to \infty$, i.e., the case of an isolated nanowire. When the gap is sufficiently large and even $\delta \to \infty$, the Coulomb interaction between the excess charges on the two nanowires diminishes, resulting in an angle-independent d parameter shown in Fig. 3(a). When further decreasing the gap from 1.5 nm to 0.5 nm, the d parameter curve of the P + N case shows a clear transition from flat to steep because the excess charge localized in the gap region is more sensitive to the gap change when the gap is small. In contrast, the variation of the d parameter when tuning the gap from 1.5 nm to 0.5 nm for the P + P and N + N cases is much smaller.

After studying the ground state, we move on to the excited state following the applied impulsive perturbation [38]. The absorption cross section, induced electron distribution, and electric field enhancement are presented in Fig. 4. A noticeable blueshift of the lower dipole mode (the first resonance peak in the absorption spectrum), as the gap size increases from $\delta = 0.5$ nm to $\delta = 1$ nm, is visible in the absorption cross sections reported in Figs. 4(a) and 4(d), a phenomenon well explained by classical electromagnetism [44]. In addition, the dipole plasmon resonance frequency of the positively (negatively) charged nanowire dimer experiences a blueshift (redshift) concerning the charge-neutral case. This resonance shift in the absorption cross section due to the excess charge agrees with the previous works [16,17], and it is attributed to the distribution of the screening charges relative to the sharp edge of the jellium background. Adding (removing) electrons to the dimer increases (decreases) the spill out of the electrons. As shown in Figs. 4(b) and 4(e), the neutral, P + P, and N + N cases all give an antisymmetric profile of the induced electron distributions. Since, in the P + N case, the symmetry of the potential barrier across the gap is broken, an asymmetric induced electron distribution is observed. The degree of asymmetry decreases as the gap size is increased from 0.5 nm to 1 nm due to a weaker electrostatic interaction between two charged nanowires.

The electric field enhancement for the dipole mode of different charged dimers is illustrated in Figs. 4(c) and 4(f) for gap size of $\delta = 0.5$ nm and $\delta = 1$ nm, respectively. The asymmetric induced electron distribution for the P + N case also leads to an asymmetric near field. In Table II, we

TABLE II. $|E/E_0|$ in the middle of the gap.

Dimer	0.5 nm	1 nm
Neutral	22.6	16.2
P+P	23.4	16.1
N+N	21.2	16.0
P+N	20.5	16.1

summarize the field enhancement, defined as $|E/E_0|$, observed at the center of the gap. As expected, a smaller gap gives a larger field enhancement due to a stronger confinement [44]. Moreover, the nanowire dimer with opposite charging gives the smallest field enhancement compared with the other charging configurations in the case of $\delta = 0.5$ nm. This decreased field enhancement originates from the charge transfer between two nanowires [45,46], screening the electric field in the gap. The asymmetric potential barrier facilitates the formation of current flow in the gap, similar to what was observed in previous studies when an external dc bias across a narrow gap was applied [13]. Furthermore, field enhancements for different charging configurations are nearly identical for a larger gap with $\delta = 1$ nm. This smaller discrepancy between P + N and other cases is attributed to a weaker charge transfer shown in Fig. 1(f).

IV. CONCLUSION

We have modeled the charging effect in plasmonic nanowire dimers using DFT and real-time TDDFT calculations. An external potential is first applied to polarize the dimers and then it is smoothly removed to obtain two oppositely charged nanowires while the dimer is overall neutral. The excess charge distribution of the oppositely charged dimer breaks the parity symmetry of the potential barrier, facilitating charge transfer across the gap. In addition, the access charges have been shown to strongly modulate the absorption spectrum, the induced electron profile, and the field enhancement in the gap. Furthermore, the nonuniform excess charge distribution indicates that an analytical treatment of the surface charging requires a coordinate-dependent Feibelman d parameter.

ACKNOWLEDGMENTS

We thank P. Zhang and R. Qin for the fruitful discussion. F.Y. acknowledges the financial support from the National Natural Science Foundation of China (Grant No. 12204328), Sichuan Science and Technology Program (Grant No. 2024NSFSC1351), the Fundamental Research Funds for the Central Universities, and the Science Specialty Program of Sichuan University (Grant No. 2020SCUNL210). H.Z. acknowledges the financial support from the National Natural Science Foundation of China (Grant No. 11974253) and the Science Specialty Program of Sichuan University (Grant No. 2020SCUNL210).

APPENDIX A: SIMULATION SETUP FOR DFT AND TDDFT CALCULATION

The simulation box is constructed by adding parallelepipeds, with a uniform mesh grid of 0.5 Å element size. The approximated enforced time-reversal symmetry (AETRS) algorithm is used to approximate the evolution operator in our real-time propagation and the Kohn-Sham wave functions are evolved for typically 8000 steps in time steps of 0.005 $\hbar$/eV.

APPENDIX B: NUMERICAL EVALUATION OF D PARAMETER

In the evaluation of the d parameter, a finer mesh with element size 0.2 Å is applied to obtain a smooth curve. Because of numerical discretization in the meshing, the effective jellium edge is not a perfect circle. The real jellium edge is determined by enforcing $d_{\parallel} = 0$ for the charge-neutral case as a result of charge conservation, making the radius of the nanowire an angle-dependent function $r(\theta)$.

[1] R. P. Feynman, *The Feynman Lectures on Physics* (Basic Books, New York, 1963), Vol. I.

[2] J. D. Jackson, *Classical Electrodynamics* (American Association of Physics Teachers, College Park, MD, 1999).

[3] J. A. Stratton, *Electromagnetic Theory* (John Wiley & Sons, New York, 2007), Vol. 33.

[4] S. Linic, S. Chavez, and R. Elias, Flow and extraction of energy and charge carriers in hybrid plasmonic nanostructures, Nat. Mater. **20**, 916 (2021).

[5] H. Kang, J. T. Buchman, R. S. Rodriguez, H. L. Ring, J. He, K. C. Bantz, and C. L. Haynes, Stabilization of silver and gold nanoparticles: Preservation and improvement of plasmonic functionalities, Chem. Rev. **119**, 664 (2019).

[6] Y. Wang, J. Yu, Y.-F. Mao, J. Chen, S. Wang, H.-Z. Chen, Y. Zhang, S.-Y. Wang, X. Chen, T. Li *et al.*, Stable, high-performance sodium-based plasmonic devices in the near infrared, Nature (London) **581**, 401 (2020).

[7] Y. Xu, P. Bai, X. Zhou, Y. Akimov, C. E. Png, L.-K. Ang, W. Knoll, and L. Wu, Optical refractive index sensors with plasmonic and photonic structures: Promising and inconvenient truth, Adv. Opt. Mater. **7**, 1801433 (2019).

[8] W. Jiang, B. Q. L. Low, R. Long, J. Low, H. Loh, K. Y. Tang, C. H. T. Chai, H. Zhu, H. Zhu, Z. Li *et al.*, Active site engineering on plasmonic nanostructures for efficient photocatalysis, ACS Nano **17**, 4193 (2023).

[9] S. Ezendam, M. Herran, L. Nan, C. Gruber, Y. Kang, F. Gröbmeyer, R. Lin, J. Gargiulo, A. Sousa-Castillo, and E. Cortés, Hybrid plasmonic nanomaterials for hydrogen generation and carbon dioxide reduction, ACS Energy Lett. **7**, 778 (2022).

[10] C. Novo, A. M. Funston, A. K. Gooding, and P. Mulvaney, Electrochemical charging of single gold nanorods, J. Am. Chem. Soc. **131**, 14664 (2009).

[11] C. P. Byers, H. Zhang, D. F. Swearer, M. Yorulmaz, B. S. Hoener, D. Huang, A. Hoggard, W.-S. Chang, P. Mulvaney, E. Ringe *et al.*, From tunable core-shell nanoparticles to plasmonic drawbridges: Active control of nanoparticle optical properties, Sci. Adv. **1**, e1500988 (2015).

[12] Y. Jin, L. Zhou, J. Liang, and J. Zhu, Electrochemically driven dynamic plasmonics, Adv. Photon. **3**, 044002 (2021).

[13] D. C. Marinica, M. Zapata, P. Nordlander, A. K. Kazansky, P. M. Echenique, J. Aizpurua, and A. G. Borisov, Active quantum plasmonics, Sci. Adv. **1**, e1501095 (2015).

[14] W. Li, Q. Zhou, P. Zhang, and X.-W. Chen, Direct electro plasmonic and optic modulation via a nanoscopic electron reservoir, Phys. Rev. Lett. **128**, 217401 (2022).
[15] L. Zurak, C. Wolff, J. Meier, R. Kullock, N. A. Mortensen, B. Hecht, and T. Feichtner, Direct electrical modulation of surface response in a single plasmonic nanoresonator, arXiv:2307.01423.
[16] H. M. Zapata, J. Aizpurua, A. Kazansky, and A. Borisov, Plasmon response and electron dynamics in charged metallic nanoparticles, Langmuir **32**, 2829 (2016).
[17] M. Z. Herrera, A. K. Kazansky, J. Aizpurua, and A. G. Borisov, Quantum description of the optical response of charged monolayer–thick metallic patch nanoantennas, Phys. Rev. B **95**, 245413 (2017).
[18] P. Mulvaney, J. Pérez-Juste, M. Giersig, L. M. Liz-Marzán, and C. Pecharromán, Drastic surface plasmon mode shifts in gold nanorods due to electron charging, Plasmonics **1**, 61 (2006).
[19] P. Hohenberg and W. Kohn, Inhomogeneous electron gas, Phys. Rev. **136**, B864 (1964).
[20] W. Kohn and L. J. Sham, Self-consistent equations including exchange and correlation effects, Phys. Rev. **140**, A1133 (1965).
[21] E. Runge and E. K. U. Gross, Density-functional theory for time-dependent systems, Phys. Rev. Lett. **52**, 997 (1984).
[22] A. Zangwill and P. Soven, Density-functional approach to local-field effects in finite systems: Photoabsorption in the rare gases, Phys. Rev. A **21**, 1561 (1980).
[23] W. Ekardt and Z. Penzar, Collective excitations in open-shell metal clusters: The time-dependent local-density approximation applied to the self-consistent spheroidal jellium particle, Phys. Rev. B **43**, 1322 (1991).
[24] W. Kleinig, V. Nesterenko, P.-G. Reinhard, and L. Serra, Plasmon response in K, Na and Li clusters: Systematics using the separable random-phase-approximation with pseudo-Hamiltonians, Eur. Phys. J. D **4**, 343 (1998).
[25] T. Takeuchi, M. Noda, and K. Yabana, Operation of quantum plasmonic metasurfaces using electron transport through subnanometer gaps, ACS Photon. **6**, 2517 (2019).
[26] C. Yannouleas, R. A. Broglia, M. Brack, and P. F. Bortignon, Fragmentation of the photoabsorption strength in neutral and charged metal microclusters, Phys. Rev. Lett. **63**, 255 (1989).
[27] C. Yannouleas, From the cationic to the anionic alkali clusters: How the photoabsorption depends upon the total charge, Chem. Phys. Lett. **193**, 587 (1992).
[28] C. Yannouleas, Microscopic description of the surface dipole plasmon in large Na_N clusters ($950 \lesssim n \lesssim 12050$), Phys. Rev. B **58**, 6748 (1998).
[29] D. C. Marinica, A. K. Kazansky, P. Nordlander, J. Aizpurua, and A. G. Borisov, Quantum plasmonics: Nonlinear effects in the field enhancement of a plasmonic nanoparticle dimer, Nano Lett. **12**, 1333 (2012).
[30] R. Esteban, A. G. Borisov, P. Nordlander, and J. Aizpurua, Bridging quantum and classical plasmonics with a quantum-corrected model, Nat. Commun. **3**, 825 (2012).
[31] T. V. Teperik, P. Nordlander, J. Aizpurua, and A. G. Borisov, Robust subnanometric plasmon ruler by rescaling of the nonlocal optical response, Phys. Rev. Lett. **110**, 263901 (2013).
[32] L. Stella, P. Zhang, F. García-Vidal, A. Rubio, and P. García-González, Performance of nonlocal optics when applied to plasmonic nanostructures, J. Phys. Chem. C **117**, 8941 (2013).
[33] P. Zhang, J. Feist, A. Rubio, P. García-González, and F. J. García-Vidal, *Ab initio* nanoplasmonics: The impact of atomic structure, Phys. Rev. B **90**, 161407(R) (2014).
[34] W. Yan, M. Wubs, and N. Asger Mortensen, Projected dipole model for quantum plasmonics, Phys. Rev. Lett. **115**, 137403 (2015).
[35] K. Yabana and G. F. Bertsch, Time-dependent local-density approximation in real time, Phys. Rev. B **54**, 4484 (1996).
[36] A. Castro, H. Appel, M. Oliveira, C. A. Rozzi, X. Andrade, F. Lorenzen, M. A. Marques, E. Gross, and A. Rubio, *octopus:* a tool for the application of time-dependent density functional theory, Phys. Status Solidi B **243**, 2465 (2006).
[37] X. Andrade, D. Strubbe, U. De Giovannini, A. H. Larsen, M. J. Oliveira, J. Alberdi-Rodriguez, A. Varas, I. Theophilou, N. Helbig, M. J. Verstraete *et al.*, Real-space grids and the Octopus code as tools for the development of new simulation approaches for electronic systems, Phys. Chem. Chem. Phys. **17**, 31371 (2015).
[38] A. Varas, P. García-González, J. Feist, F. García-Vidal, and A. Rubio, Quantum plasmonics: From jellium models to *ab initio* calculations, Nanophotonics **5**, 409 (2016).
[39] J. P. Perdew and A. Zunger, Self-interaction correction to density-functional approximations for many-electron systems, Phys. Rev. B **23**, 5048 (1981).
[40] A. Liebsch, *Electronic Excitations at Metal Surfaces* (Springer Science & Business Media, New York, 1997).
[41] N. W. Ashcroft and N. D. Mermin, *Solid State Physics* (Cengage Learning, Boston, 2022).
[42] P. J. Feibelman, Surface electromagnetic fields, Prog. Surf. Sci. **12**, 287 (1982).
[43] F. Yang and K. Ding, Transformation optics approach to mesoscopic plasmonics, Phys. Rev. B **105**, L121410 (2022).
[44] A. Aubry, D. Y. Lei, S. A. Maier, and J. B. Pendry, Interaction between plasmonic nanoparticles revisited with transformation optics, Phys. Rev. Lett. **105**, 233901 (2010).
[45] K. J. Savage, M. M. Hawkeye, R. Esteban, A. G. Borisov, J. Aizpurua, and J. J. Baumberg, Revealing the quantum regime in tunnelling plasmonics, Nature (London) **491**, 574 (2012).
[46] J. A. Scholl, A. García-Etxarri, A. L. Koh, and J. A. Dionne, Observation of quantum tunneling between two plasmonic nanoparticles, Nano Lett. **13**, 564 (2013).